Remarkable nucleation and growth of ultrafine particles from vehicular exhaust

Song Guo[a,1], Min Hu[a,1,2], Jianfei Peng[b,c,1,3], Zhijun Wu[a], Misti L. Zamora[b,c,1,4], Dongjie Shang[a], Zhuofei Du[a], Jing Zheng[a], Xin Fang[a], Rongzhi Tang[a], Yusheng Wu[a], Limin Zeng[a], Shijin Shuai[d], Wenbin Zhang[d], Yuan Wang[e], Yuemeng Ji[b,c,f], Yixin Li[b,c], Annie L. Zhang[g], Weigang Wang[b,c,h], Fang Zhang[b,c,i], Jiayun Zhao[b,c], Xiaoli Gong[b,c,j], Chunyu Wang[b,c,k], Mario J. Molina[l,2], and Renyi Zhang[b,c,2]

[a]State Key Joint Laboratory of Environmental Simulation and Pollution Control, College of Environmental Sciences and Engineering, Peking University, 100871 Beijing, China; [b]Department of Atmospheric Sciences, Texas A&M University, College Station, TX 77843; [c]Department of Chemistry, Texas A&M University, College Station, TX 77843; [d]State Key Laboratory of Automotive Safety and Energy, Tsinghua University, 100084 Beijing, China; [e]Division of Geological and Planetary Sciences, California Institute of Technology, Pasadena, CA 91125; [f]Guangzhou Key Laboratory of Environmental Catalysis and Pollution Control, School of Environmental Science and Engineering, Institute of Environmental Health and Pollution Control, Guangdong University of Technology, 510006 Guangzhou, China; [g]Department of Chemistry, College of Natural Sciences, The University of Texas at Austin, Austin, TX 78712; [h]State Key Laboratory for Structural Chemistry of Unstable and Stable Species, Beijing National Laboratory for Molecular Sciences, Institute of Chemistry, Chinese Academy of Sciences,100190 Beijing, China; [i]State Key Laboratory of Earth Surface Processes and Resource Ecology, College of Global Change and Earth System Science, Beijing Normal University, 100875 Beijing, China; [j]College of Electronic Information, Hangzhou Dianzi University, 310018 Hangzhou, Zhejiang, China; [k]School of Information Science and Technology, University of Science and Technology of China, 230026 Hefei, Anhui, China; and [l]Department of Chemistry and Biochemistry, University of California San Diego, La Jolla, CA 92093

Contributed by Mario J. Molina, December 19, 2019 (sent for review September 23, 2019; reviewed by Robert L. McGraw and Fangqun Yu)

High levels of ultrafine particles (UFPs; diameter of less than 50 nm) are frequently produced from new particle formation under urban conditions, with profound implications on human health, weather, and climate. However, the fundamental mechanisms of new particle formation remain elusive, and few experimental studies have realistically replicated the relevant atmospheric conditions. Previous experimental studies simulated oxidation of one compound or a mixture of a few compounds, and extrapolation of the laboratory results to chemically complex air was uncertain. Here, we show striking formation of UFPs in urban air from combining ambient and chamber measurements. By capturing the ambient conditions (i.e., temperature, relative humidity, sunlight, and the types and abundances of chemical species), we elucidate the roles of existing particles, photochemistry, and synergy of multipollutants in new particle formation. Aerosol nucleation in urban air is limited by existing particles but negligibly by nitrogen oxides. Photooxidation of vehicular exhaust yields abundant precursors, and organics, rather than sulfuric acid or base species, dominate formation of UFPs under urban conditions. Recognition of this source of UFPs is essential to assessing their impacts and developing mitigation policies. Our results imply that reduction of primary particles or removal of existing particles without simultaneously limiting organics from automobile emissions is ineffective and can even exacerbate this problem.

new particle formation | nucleation | ultrafine particles | growth | organics

High levels of ultrafine particles (UFPs; diameter smaller than 50 nm) are produced during new particle formation (NPF) events, representing a significant source of tropospheric fine aerosols and cloud condensation nuclei (1–9). NPF occurs via two distinct stages (i.e., nucleation to form a critical nucleus and its subsequent growth to freshly nucleated particles of 1 to 3 nm, which are associated with a thermodynamic and a kinetic barrier, respectively) (1). Freshly nucleated particles are subjected to collision loss among themselves, coagulation loss by existing particles, or growth to nucleation-mode particles (>3 nm). Under favorable atmospheric conditions, nucleation-mode particles grow continuously to submicrometer (i.e., fine particulate matter smaller than 2.5 μm [$PM_{2.5}$]) or cloud condensation nuclei. Atmospheric measurements have shown ubiquitous NPF events under both pristine and urban conditions (1–5, 8), with important societal implications (10–14). For example, high levels of UFPs formed under urban environments have been attributed to substantial enhancement in convection and precipitation (11). Also, recent studies have demonstrated that maternal exposure to UFPs results in pulmonary immunosuppression and birth defects and fatalities in offspring, highlighting the necessity of accounting for these smallest particles when formulating air quality standards (13, 14).

Measurements of urban NPF exhibit distinct characteristics worldwide (8), but the cause for the variability remains mysterious (15). Various species have been suggested to account for nucleation and growth of UFPs, including sulfuric acid (H_2SO_4),

Significance

High concentrations of ultrafine particles (UFPs), approaching 1 million/cm^3, are frequently produced from new particle formation under urban environments, but the fundamental mechanisms regulating nucleation and growth for UFPs are poorly understood. From simultaneous ambient and environmental chamber measurements, we demonstrate remarkable formation of UFPs from urban traffic emissions. By replicating ambient conditions using an environmental chamber method, we elucidate the roles of existing particles, photochemistry, and synergy of multipollutant photooxidation in nucleation and growth of UFPs. Our results reveal that synergetic oxidation of vehicular exhaust leads to efficient formation of UFPs under urban conditions. Recognition of this large urban source for UFPs is essential to accurately assessing their impacts and to effectively developing mitigation policies.

Author contributions: S.G., M.H., and R.Z. designed research; S.G., M.H., J.P., Z.W., M.L.Z., D.S., Z.D., J. Zheng, X.F., R.T., Y.W., S.S., W.Z., Y.W., Y.J., Y.L., W.W., F.Z., J. Zhao, X.G., C.W., and R.Z. performed research; S.S., M.J.M., and R.Z. contributed new reagents/analytic tools; S.G., M.H., J.P., Z.W., M.L.Z., L.Z., S.S., Y.W., A.L.Z., M.J.M., and R.Z. analyzed data; and S.G., M.H., A.L.Z., and R.Z. wrote the paper.

Reviewers: R.L.M., Brookhaven National Laboratory; and F.Y., State University of New York at Albany.

The authors declare no competing interest.

[1]S.G., M.H., J.P., and M.L.Z. contributed equally to this work.

[2]To whom correspondence may be addressed. Email: minhu@pku.edu.cn, mjmolina@ucsd.edu, or renyi-zhang@tamu.edu.

[3]Present addresses: Center for Urban Transport Emission Research and State Environmental Protection Key Laboratory of Urban Ambient Air Particulate Matter Pollution Prevention and Control, College of Environmental Science and Engineering, Nankai University, Tianjin 300071, China.

[4]Present address: Department of Environmental Health and Engineering, Bloomberg School of Public Health, Johns Hopkins University, Baltimore, MD 21205.

This article contains supporting information online at https://www.pnas.org/lookup/suppl/doi:10.1073/pnas.1916366117/-/DCSupplemental.

First published February 3, 2020.

organic acids from oxidation of volatile organic compounds (VOCs), ammonia/amines, and ions (1–6, 16–22). However, there is a lack of consistent mechanisms to explain NPF under diverse atmospheric conditions (1, 8). Despite intensive effort in developing state-of-the-art instrumentations to investigate NPF in laboratory studies, available analytical methods have been unable to replicate the atmospheric conditions in pristine or urban air, particularly the chemical complexity (8). Another major limitation is related to the lack of chemical speciation; analytical instruments capable of unambiguously detecting the various nucleating vapors, neutral/ionic prenucleation clusters, and the chemical compositions of subnanometer particles have yet to be developed (1, 8). Previous studies showed that NPF is enhanced with coexisting H_2SO_4, base species, organic acids, and ions (2–6, 16–22) but is suppressed for oxidation of monoterpene in the presence of nitrogen oxides (NO_x) (23) or isoprene (24), indicating large synergetic effects in a chemically complex mixture. The deficiencies in understanding NPF considerably hinder effort in developing physically based models to predict atmospheric aerosol formation and to assess the impacts of UFPs on human health, weather, and climate (7, 11).

To unravel the fundamental mechanisms of nucleation and growth for UFPs, we performed three types of measurements (*Methods*), including the application of a quasiatmospheric aerosol evolution study (QUALITY) chamber (25, 26). In situ measurements of gases and aerosols were performed at a traffic-dominant urban site (2, 25, 26). In addition, QUALITY chamber experiments were performed simultaneously with the ambient measurements at this urban site. A dual-layer design of the QUALITY chamber allowed ambient gases to permeate through a Teflon membrane into a ultraviolet (UV) transmission upper reaction chamber, while ambient particles were filtrated by the membrane (*SI Appendix*, Fig. S1) (25, 26). The major advantage of this approach was in closely replicating the atmospheric conditions (i.e., temperature, relative humidity, solar radiation, gases, and their photochemistry) throughout the experiments but without the presence of preexisting particles. In addition, we evaluated NPF in an enclosed environmental chamber using vehicular exhaust from a gasoline car operating on a chassis dynamometer (*SI Appendix*, Fig. S2) (27).

NPF in Ambient Air

NPF is dependent on existing particle and photochemistry at this urban site (2). High levels of UFPs are produced in clean air but not in polluted air (Fig. 1 and *SI Appendix*, Fig. S3), with the corresponding ambient $PM_{2.5}$ levels of 2 to 20 and 78 to 128 $\mu g\ m^{-3}$, respectively (*SI Appendix*, Tables S1 and S2). NPF occurs continuously during the morning hours in clean air, and the nucleation-mode particles grow to about 20 to 30 nm within about 4 to 5 h (Fig. 1*A* and *SI Appendix*, Fig. S3 *B* and *D*), referred to as continuum NPF. In contrast, high levels of existing particles inhibit NPF in polluted air (Fig. 1*B* and *SI Appendix*, Fig. S3 *F* and *H*). The clean and polluted conditions during our measurements correspond to distinct air masses and emission characteristics, i.e., under strong northerly wind from clean areas and with low relative humidity (RH) (14 to 21%) and weak southerly wind from populated, industrial regions and with high RH (30 to 52%), respectively. Aromatic hydrocarbons represent the most abundant VOCs at this site (higher than biogenic VOCs), ranging from a few parts per billion (ppb) in clean air to up to 20 ppb in polluted air (*SI Appendix*, Figs. S4 and S5 and Tables S1 and S2). The concentrations of other primary gases range from 8 to 14 ppb and from 88 to 132 ppb for NO_x and from a few parts per billion to up to 30 ppb for SO_2 in clean and polluted air, respectively. The daily O_3 peak is 30 to 40 ppb in clean air and 10 to 20 ppb in polluted air, consistent with reduced photochemical activity in the latter. Gaseous H_2SO_4 at the site is strongly dependent on the $PM_{2.5}$ level and actinic flux, with average daily peak levels of 1×10^7 molecules cm^{-3} in clean air and 5×10^6 molecules cm^{-3} in polluted air and a

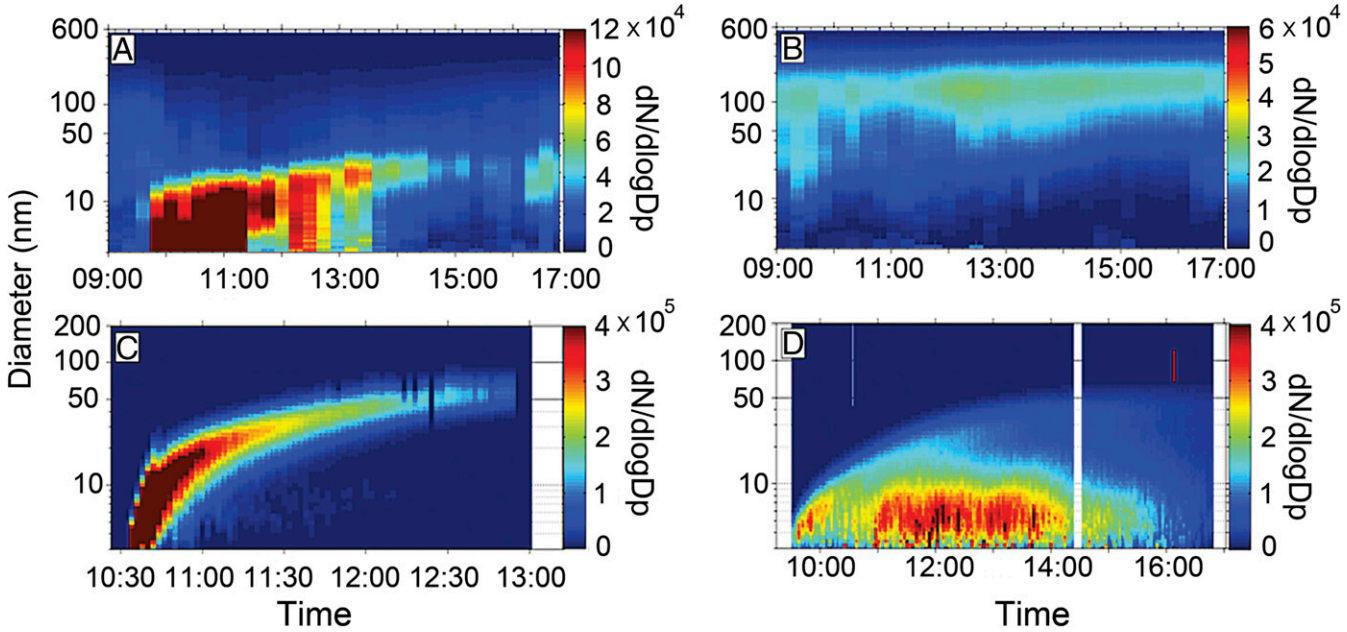

Fig. 1. Contrasting NPF between ambient air and QUALITY chamber. Particle number size distributions in ambient air (*A* and *B*) and inside the chamber (*C* and *D*) with initial filtration of ambient preexisting particles. The experiments were performed on 23 October 2013 (*A* and *C*; clean) and 8 November 2013 (*B* and *D*; polluted), corresponding to clean air (*A*) or clean chamber (*C*) and polluted air (*B*) or polluted chamber (*D*), respectively. The color contour on the right vertical axes denotes the particle number concentration (i.e., $dN/d\log D'$ [$centimeters^{-3}$], where N and D' represent the particle number and size, respectively). Detailed information on the atmospheric conditions during the ambient and chamber measurements is presented in *SI Appendix*, Figs. S4 and S5 and Tables S1 and S2.

concentration of below 10^6 molecules cm^{-3} at sunrise/sunset (3, 28). We further determined the O_3 photolysis frequency yielding an excited oxygen atom, $J(O^1D)$, which quantifies the extent and efficiency of photooxidation of primary gases to produce the precursors for NPF (1, 28, 29). The $J(O^1D)$ values range from 4.9×10^{-6} to 1.3×10^{-5} s^{-1} in clean air and from 1.8×10^{-6} to 3.4×10^{-6} s^{-1} in polluted air, inversely correlated to the $PM_{2.5}$ levels (*SI Appendix*, Tables S1 and S2). In addition, we calculated the formation rate (in the size range of 3 to 25 nm) and growth rate (*Methods*), which are relevant to nucleation and growth of UFPs, respectively. Existing particles and photochemistry regulate the formation and growth rates of UFPs. The calculated formation and growth rates range from 20 to 42 cm^{-3} s^{-1} and from 5 to 20 nm h^{-1}, respectively, during NPF in clean air. Elevated concentrations of $PM_{2.5}$ suppress NPF in polluted air because of reduced photochemistry or a large surface area of preexisting particles to capture freshly nucleated particles.

NPF in Captured Urban Air

NPF inside the QUALITY chamber is distinct from that in ambient air (Fig. 1 and *SI Appendix*, Fig. S3 and Tables S1 and S2). Noticeably, highly abundant UFPs are produced under both clean and polluted conditions inside the QUALITY chamber (Fig. 1 *C* and *D*), referred to as clean chamber and polluted chamber, respectively. UFPs typically appear within 5 to 15 min of exposing the reaction chamber to sunlight throughout daytime. In clean chamber, NPF occurs momentarily, and the nucleation-mode particles grow rapidly to about 50 nm within about 2 h, commonly known as banana NPF (Fig. 1*C* and *SI Appendix*, Fig. S3 *A* and *C*). Similar to the case in clean air (Fig. 1*A*), continuum NPF is also evident in polluted chamber, albeit with a much slower growth (i.e., size not exceeding 20 nm) (*SI Appendix*, Fig. S3 *E* and *G*). In clean chamber, efficient nucleation and growth of UFPs are also reflected by the large formation (82 to 332 cm^{-3} s^{-1}) and growth (15 to 79 nm h^{-1}) rates, respectively. In polluted chamber, efficient nucleation and slow growth are evident from the large formation rates (79 to 166 cm^{-3} s^{-1}) and small growth rates (5 to 7 nm h^{-1}), respectively. The formation rates in clean and polluted chambers are nearly comparable, and both are much larger than those in clean air (21 to 41 cm^{-3} s^{-1}). The growth rates are much larger in clean chamber than in polluted chamber but are nearly comparable in clean air and in polluted chamber (6 to 20 cm^{-3} s^{-1}). The $J(O^1D)$ values between clean and polluted chambers are different and affect distinctly the formation and growth rates. In polluted chamber, elevated levels of ambient $PM_{2.5}$ are responsible for the low growth rates (*SI Appendix*, Fig. S4 and Table S1) but impact negligibly the formation rates. Even under extremely polluted conditions, photochemistry is still adequate for NPF, albeit with slow growth rates (*SI Appendix*, Table S2). The banana NPF is characterized by both large formation and growth rates in contrast to the continuum NPF with low growth rates (<20 nm h^{-1}) (*SI Appendix*, Tables S1 and S2). Furthermore, NO_x does not influence NPF at this urban site since NPF is consistently observed inside the QUALITY chamber over a large NO_x range, i.e., from 8 to 14 ppb in clean air and from 88 to 132 ppb in polluted air.

Masked NPF in Polluted Air

To differentiate the roles of existing particles and photochemistry in NPF, we performed additional QUALITY chamber experiments without initial filtration of ambient preexisting particles under the polluted conditions. Ambient air was initially pumped into the reaction chamber through an air-open port to bypass the membrane. After injection of ambient air, the reaction chamber was sealed and pumped by a constant flow (~10 L min^{-1}) to gradually remove preexisting particles, while ambient gases penetrated through the membrane to continuously replicate the atmospheric conditions (Fig. 2 and *SI Appendix*, Fig. S6 and Table S2). There are clear distinctions in the chamber experiments with and without initial filtration of ambient preexisting particles. Without filtration, NPF exhibits a significant delay of about an hour and occurs repeatedly (Fig. 2*A*), in contrast to instantaneous appearance of UFPs with filtration (Fig. 1*D*). Also, the particle number concentration decreases and increases alternatively inside the reaction chamber because of constant removal of existing (nucleation-mode and ambient preexisting) particles and reoccurrence of NPF, while the particle surface area decreases monotonically because of the removal of large preexisting particles (Fig. 2*B* and *SI Appendix*, Fig. S6*B*). The onset for each NPF (Fig. 2*A* and *SI Appendix*, Fig. S6*A*) is dependent on the particle number concentration and surface area (i.e., sizes larger than 3 nm); there is an anticorrelation between the two, i.e., occurring at a lower number concentration with a larger surface area but at a higher number concentration with a smaller surface area (Fig. 2*C*). In addition to coagulation by existing particles, freshly nucleated particles possess large diffusional speed, resulting in significant collision coagulation among themselves (*SI Appendix*, Table S3). For the experiments without initial filtration, the particle surface area decreases continuously because of removal of preexisting particles, and NPF occurs consecutively at increasing particle number concentration (Fig. 2*B* and *SI Appendix*, Fig. S6*B*). The impact of photochemistry on the growth of UFPs is further illustrated by the positive correlation between the growth rate and $J(O^1D)$ (Fig. 2*D*): the growth rate increases from 10 to 80 nm h^{-1} with $J(O^1D)$ increasing from 3 to 14 s^{-1}. For the experiments without filtration, an inefficient photochemistry results in low growth rates (*SI Appendix*, Table S2), and only continuum NPF occurs, similar to those in clean air and in polluted chamber (Fig. 1 and *SI Appendix*, Fig. S3).

Linking NPF to Vehicle-Emitted Organics

We inferred the chemical composition of UFPs inside the QUALITY chamber from size-resolved and temporally resolved particle effective density and hygroscopicity (Fig. 3 *A* and *B* and *SI Appendix*, Fig. S7 *A* and *B*). Both effective density and hygroscopicity increase with the particle size, i.e., from 1.03 to 1.16 g cm^{-3} for 50 to 62 nm and from 1.05 to 1.15 for 21 to 62 nm, respectively. The evolution in both quantities reflects an organics-dominated ingredient of UFPs and an increasing inorganic fraction with the particle growth (2, 30). The initial growth of UFPs is dominated by nonvolatile organics formed from VOC oxidation or via multiphase reaction since H_2SO_4 production from the reaction of SO_2 with hydroxyl radical is a slow process (1). It is also evident that the chemical species responsible for the nucleation and growth of UFPs are distinct, relevant to the processes to overcome the thermodynamic and kinetic barriers for NPF (15). Specifically, the organics governing the nucleation and growth likely correspond to less and highly oxidized forms, respectively, i.e., with high-reactivity for hydrogen-bonding formation but low-volatility for particle growth (1, 8). In addition, a high-resolution time-of-flight aerosol mass spectrometer (HR-ToF-AMS) (31) was used to measure the chemical compositions (Fig. 3 *C* and *D*) inside the QUALITY chamber for particles with the mean sizes of 30 and 60 nm (*SI Appendix*, Fig. S7 *C* and *D*). The measurements by the HR-ToF-AMS show large organic mass fractions of 87% (89%) for 30-nm particles and 62% (53%) for 62-nm particles, also representative of an organic-dominant composition for fine-mode aerosols. The nitrate fraction is nonnegligible for small particles and increases for large particles, and the mass fractions of sulfate and ammonium are small for small particles and increase for large particles; both are characteristic of urban traffic-related fine aerosols (2).

To assess NPF from traffic emissions, we conducted complementary experiments by introducing gasoline vehicular exhaust (27) into an enclosed environmental chamber (i.e., without gas exchange between the chamber and ambient air). While many

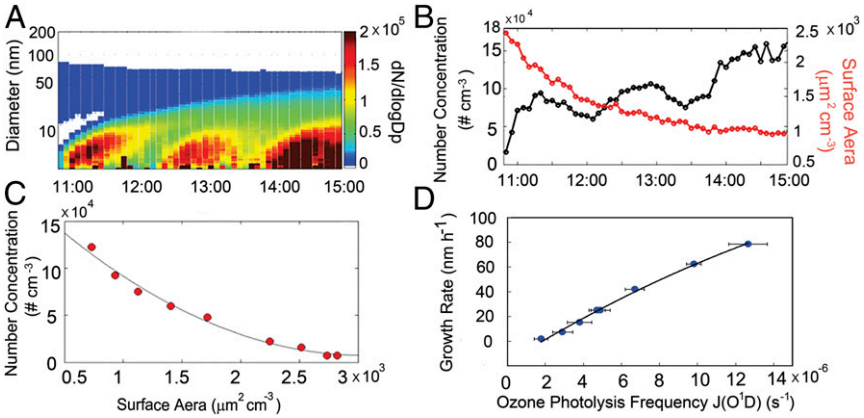

Fig. 2. Effects of preexisting particles and photochemistry. (*A*) Particle number size distributions inside the QUALITY chamber for an experiment without initial filtration of ambient preexisting particles on a polluted day (5 November 2013). (*B*) Evolution in the particle number concentration and surface area for the experiment in *A*. (*C*) Correlation between the particle number concentration and surface area at the onset of NPF for all experiments conducted on polluted days without initial filtration of ambient preexisting particles (*SI Appendix*, Table S2). (*D*) Correlation between growth rate and $J(O^1D)$ for all experiments with initial filtration of ambient preexisting particles (*SI Appendix*, Table S1).

previous studies examined the contributions of vehicular exhaust to secondary organic aerosol formation (27), few focused on NPF. Gases from the vehicular exhaust were diluted to atmospherically relevant levels in the chamber, and all experiments using vehicular exhaust were performed under the clean conditions. Banana NPF is identified from all experiments using gasoline exhaust (Fig. 3*E* and *SI Appendix*, Fig. S8), i.e., occurring momentarily after exposing the chamber to sunlight and growing rapidly to larger sizes of 100 to 200 nm. The formation and growth rates from gasoline exhaust range from 15 to 134 cm^{-3} s^{-1} and from 50 to 62 nm h^{-1}, respectively, with the low and high values corresponding to the experiments without and with addition of an initial O_3 concentration to promote photochemistry (i.e., 0 and 80 ppb O_3 in *SI Appendix*, Fig. S8 *A* and *B*), respectively. Measurements of gaseous species inside the chamber show high levels of aromatics, including toluene and C8 and C9 aromatics (*SI Appendix*, Fig. S9), but negligible SO_2 (*SI Appendix*, Fig. S8*D*). In addition, HR-ToF-AMS measurements of the smallest detectable particles (about 50 nm) indicate an exclusive presence of organics along with a trace amount of nitrate but no measurable sulfate or ammonium (i.e., at levels below the instrument detection limit) (*SI Appendix*, Fig. S8*E*). Furthermore, the NO_x level is high for the chamber measurements using vehicular exhaust (over 100 ppb) (*SI Appendix*, Fig. S8*C*), also indicating a negligibly suppressing effect.

Discussion

Our ambient measurements at this traffic-dominant urban site show that NPF occurs consistently under clean conditions, consistent with many previous studies (1–3, 16). For example, the frequency percentages of NPF events at this site are 50, 20, 35, and 45% in the spring, summer, fall, and winter, respectively (1, 2). Typically, wind circulation at this location exhibits a periodic cycle of 4 to 7 d during all seasons, which is also reflected by a similar clean-to-polluted cycle in $PM_{2.5}$ concentrations (2). The persistent occurrence of UFPs observed in clean air and inside the QUALITY chamber from this work and the previous studies (1–3, 16) indicates that RH, temperature, or NO_x plays a negligible role in NPF at this site. While NPF in ambient air mainly exhibits the banana characteristic during our measurement period, both NPF types have been observed at this urban site (1–3, 16). The occurrence of banana or continuum NPF relies on the number concentration and surface area of existing particles. The banana NPF (Fig. 1*C* and *SI Appendix*, S3 *A* and *C*) is characterized by the largest formation and growth rates (*SI Appendix*, Tables S1 and S2) under the cleanest conditions. With very low levels of existing particles and efficient photochemistry (such as in clean chamber), rapid growth of the nucleation-mode particles increases the surface area to effectively capture freshly nucleated particles. Hence, banana NPF is resulted from the suppressing effect by rapidly grown nucleation-mode particles. On the other hand, continuum NPF occurs at low to intermediate levels of ambient $PM_{2.5}$ without significant capture of freshly nucleated particles and at a low growth rate without rapid increase in the surface area of nucleation-mode particles. In addition, photooxidation of vehicular exhaust (dominantly aromatic VOCs) yields abundant precursors for nucleation and growth of UFPs (29, 32) as demonstrated in our three different types of measurements. Our ambient and chamber measurements are representative of typical urban environments worldwide (8) since the gasoline fleet of the commonly used vehicle model in China is equivalent to those in Europe and the United States (27). We conclude that NPF under urban environments is mainly driven by organics from local traffic emissions.

Although we are unable to differentiate the role of organics from those of H_2SO_4 and base species in the initial formation of prenucleation clusters (1), it is implausible that H_2SO_4 or ammonia/amines, rather than organics, dominate NPF in our study. The sources and abundances of H_2SO_4 and ammonia/amines are highly variable at this site. NPF inside the QUALITY chamber occurs throughout the daytime when exposing the reaction chamber to sunlight and under both clean and polluted conditions in contrast to the H_2SO_4 concentration that varies diurnally (by a factor of more than an order of magnitude) and with the $PM_{2.5}$ level (by a factor of two between clean and polluted air) (33). In addition, the formation and growth rates in clean air and inside the QUALITY chamber (Figs. 1 and 2 and *SI Appendix*, Tables S1 and S2) are comparable with those of the experiments using gasoline exhaust with negligible H_2SO_4 ($<5 \times 10^5$ cm^{-3}). Oxidation of VOCs is known to yield abundant organic acids, which have been suggested to contribute to aerosol nucleation (1, 9, 17, 18). Clearly, an unambiguous revelation of the identities of the chemicals contributing to the very first step of NPF ultimately waits for the advent of instrumentation to directly measure the chemical compositions of subnanometer particles.

Our work elucidates the atmospheric conditions regulating NPF (Fig. 4). NPF is dependent on preexisting particles and photochemistry, both of which impact the formation and growth rates. Synergetic photooxidation of vehicular exhaust yields abundant precursors for efficient nucleation and growth of UFPs. Under urban environments, elevated preexisting particles considerably mask NPF. Our results provide key insights into the

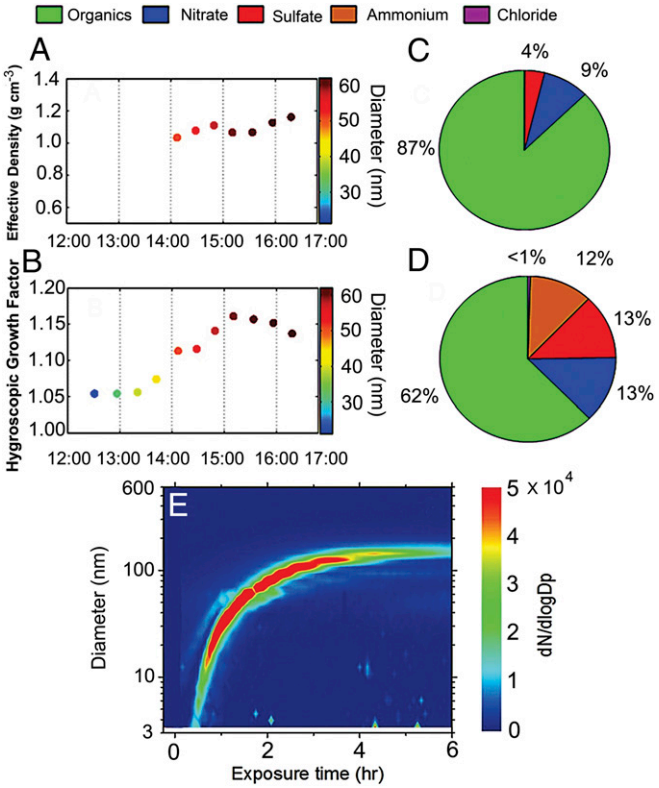

Fig. 3. Linking UFPs to vehicular exhaust. (*A* and *B*) Size-resolved particle effective density (*A*) and hygroscopicity (*B*) of nucleation-mode particles inside the QUALITY chamber. The color contour on the right vertical axes denotes the particle size (nanometers). (*C* and *D*) Particle chemical compositions inside the chamber measured by HR-ToF-AMS with the mean diameters of 30 (*C*) and 62 nm (*D*), respectively. The color legends on the top represent the chemical compositions (i.e., green for organics, blue for nitrate, red for sulfate, orange for ammonium, and purple for chloride). The experiments in *A*–*D* were performed on 23 October 2013 (clean). (*E*) Particle number size distributions for NPF inside an enclosed environmental chamber using gasoline vehicle exhaust. The color contour denotes the particle number concentration on the right vertical axis.

controversial subject of NPF under urban environments (1, 8, 34), showing that 1) aromatic VOCs from vehicular exhaust, rather than H_2SO_4 or base species, dominate the nucleation and growth of UFPs, 2) elevated concentration of NO_x exhibits a negligibly suppressing effect on NPF, 3) reduced UV radiation under hazy conditions restricts significantly the growth, but negligibly the nucleation of UFPs, and 4) the organics contributing to nucleation and growth of UFPs correspond to less and highly oxidized forms, respectively, likely with high-reactivity to form hydrogen-bonding and low-volatility to promote particle growth.

This significant source of urban UFPs is currently unaccounted for when assessing and predicting the impacts on human health, weather, and climate (8, 11). For example, highly elevated UFPs, approaching 1 million particles per cubic centimeter (Fig. 1 and *SI Appendix*, Fig. S3) (2), produced from NPF have potentially far-reaching human health outcomes (13, 14). The adverse health effects of highly elevated UFPs have yet to be carefully considered in developing air quality standards (1, 13, 14). Furthermore, our results reveal that remedy to UFPs in urban cities may not be achievable without controlling traffic emissions. Specifically, regulatory measures to mitigate emissions of primary particles or to remove preexisting particles without simultaneously reducing VOCs from automobile emissions are ineffective and can even exacerbate this problem considering the inhibitive role of preexisting particles in NPF.

Methods

Ambient Measurements. Atmospheric measurements were performed at a traffic-dominant urban site of Peking University Atmosphere Environment Monitoring Station (PKUERS) (2). During our measurement period, there was a periodic wind circulation of 4 to 7 d, which was also accompanied by a similar clean-to-hazy cycle in $PM_{2.5}$ concentrations (2). Strong northwesterly/northeasterly wind from less populated mountainous areas was most frequent during the clean period, whereas weak southerly wind from heavily populated, industrial regions was most prevalent during the hazy period. A suite of state-of-the-art instruments was deployed to simultaneously measure the particle number size distribution, chemical composition, and size-resolved effective density and hygroscopicity. A combined nanoscanning mobility particle sizer (nano-SMPS) and standard SMPS was deployed to measure the particle number size distributions. An Aerodyne HR-ToF-AMS was used to measure the chemical compositions of submicrometer particles. The size-resolved particle density and hygroscopicity were measured using a differential mobility analyzer–aerosol particle mass analyzer system and a hygroscopic tandem differential mobility analyzer (35–37). A proton transfer reaction–mass spectrometer (PTR-MS) was used to measure VOCs (38). A series of gaseous pollutant analyzers was used to measure SO_2, CO, NO-NO_2, and O_3.

QUALITY Chamber Experiments. Simultaneous chamber experiments at the PKUERS site were performed using a 1.2-m^3 portable QUALITY chamber that captured ambient conditions (i.e., gaseous concentrations, temperature, relative humidity, and solar radiation) but in the absence of preexisting particles. A detailed description and calibration of the QUALITY chamber have been provided elsewhere (25, 26). Briefly, the QUALITY chamber was composed of a lower flow chamber, where ambient air was pulled through continuously at a flow of 30 L min^{-1}, and an upper reaction chamber, where the NPF experiments were conducted. The two chambers were separated by a 5-mm-thick Teflon membrane, which allowed exchange of ambient gases from the flow chamber to the reaction chamber. The permeability of the membrane was greater than 90% for most VOCs and other gaseous pollutants (i.e., SO_2, NO_x, O_3, and CO). Ambient particles in contrast were prevented from penetration into the reaction chamber, and the filtration efficiency of the membrane was over 99.5% for particles larger than 15 nm. The differences in temperature and RH between ambient air and the reaction chamber were within ±1 °C and ±3%, respectively. The QUALITY chamber was shown to well reproduce photochemical production of low-volatility species, such as sulfuric acid (26). Typically, the sulfuric acid

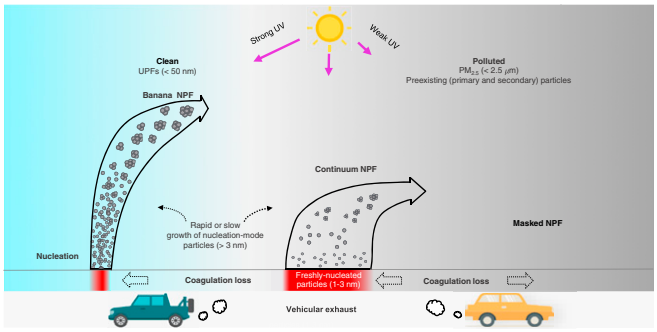

Fig. 4. Unraveling NPF in urban air. Photochemical oxidation of vehicular exhaust (i.e., aromatic VOCs) yields abundant precursors for efficient nucleation and growth of UFPs. Nucleation produces freshly nucleated particles, which are subjected to coagulation capture by existing particles or growth to nucleation-mode particles (>3 nm). Under clean conditions with the lowest levels of preexisting particles and strong UV radiation, momentary nucleation of freshly nucleated particles (marked by red color) and rapid growth of nucleation-mode particles result in banana NPF. With low to intermediate levels of preexisting particles, continuous nucleation and relatively slow growth of nucleation-mode particles result in continuum NPF. Nucleation is suppressed by coagulation loss of freshly nucleated particles by nucleation-mode particles or preexisting particles (horizontal dashed arrows). During pollution evolution (from left to right), nucleation-mode particles successively grow to larger sizes to contribute to UFPs or $PM_{2.5}$. Under polluted conditions, preexisting (secondary and primary) particles inhibit nucleation, leading to masked NPF, although photochemistry is still sufficient for nucleation (arrows with dashed lines).

concentration measured inside the QUALITY chamber was lower than that in ambient air by a factor of two to four.

Before each experiment, the reaction chamber was purged with zero air. About 10 L min^{-1} of zero air from a zero-air generator (Thermo Scientific 111) passed through the charcoal denuder and then, was continuously introduced into the reaction chamber for at least 24 h. The chamber was covered with two layers of anti-UV cloth to shield the chamber from sunlight prior to each measurement. During the experiments, ambient air continuously passed through the membrane from the flow to reaction chambers to ensure that gas concentrations in the reaction chamber were similar to those in ambient air. After 2 h of exchange of ambient gases into the reaction chamber, the chamber was uncovered and exposed to the sunlight. *SI Appendix*, Fig. S1 shows a schematic of the chamber setup. The QUALITY chamber was thoroughly evaluated for potential interference by impurities as also described in our previous publications (25, 26). Briefly, the levels of H_2SO_4, ammonia, and amines were found to be below the detection limits (i.e., less than 5×10^5 molecules cm^{-3}) using ion drift–chemical ionization mass spectrometry (28). In addition, we performed additional experiments by filling the QUALITY chamber with zero air and then exposing the chamber to sunlight under clean conditions: NPF inside the chamber was negligible, with a formation rate (*FR*) of much less than 1 cm^{-3} s^{-1}. The particle wall loss rate in the QUALITY chamber was measured as 5×10^{-5} s^{-1}, corresponding to a half-lifetime of about 3.5 h (26). Based on this loss rate, the influence of wall loss on *FR* was estimated to be smaller than 2%.

To further evaluate the factors regulating NPF, additional chamber experiments were performed by introducing ambient air into the reaction chamber without initial filtration of preexisting particles on hazy days. Prior to each of these experiments, ambient air was pumped into the reaction chamber for 1 h without filtration of preexisting particles. After introduction of ambient air, the reaction chamber was closed to and allowed for exchange of gases between the flow and reaction chambers. NPF experiment was started by pumping the reaction chamber with a constant flow (~10 L min^{-1}; i.e., the same flow rate for the exchange between the flow and reaction chambers). Thus, preexisting particles inside the reaction chamber were continuously removed, while the reaction chamber continuously replicated the ambient conditions.

Gasoline Vehicle Experiments. Vehicular exhaust experiments were conducted by combining the chassis dynamometer system (Burke E. Porter Machinery Company) and an outdoor enclosed environmental chamber (*SI Appendix*, Fig. S2) similarly to that described elsewhere (27). The chosen gasoline fleet was a commonly used vehicle model in China that was certified to the China IV emission standard and equivalent to Euro 4. The gasoline used in the experiments was a low-sulfur fuel according to the China V gasoline standard. The fleet was driven using a cold-start cycle to better simulate the urban driving conditions in Beijing. Gasoline vehicle exhaust was first diluted to 5.5 m^3 min^{-1} by a constant volume sampler (CVS). Approximately 5 L of diluted exhaust from the CVS was then introduced into the chamber, where the exhaust was further diluted with the preexisting zero air (*SI Appendix*, Fig. S2). The average dilution factor was ~20 in the CVS and 15 in the chamber.

Prior to each experiment, the chamber was covered with two layers of anti-UV cloth to shield the chamber from sunlight and flushed by zero air with a flow rate of 10 L min^{-1} for more than 48 h to ensure clean conditions. After the gasoline exhaust was introduced into the chamber, the anti-UV cloth was removed, and the chamber was exposed to sunlight. Particle number distributions, chemical compositions, and concentrations of inorganic and organic gases inside the chamber were measured by SMPS, HR-ToF-AMS, PTR-MS, and several gas monitors (Thermo Inc.), respectively. Zero airflow was connected to the chamber over the entire experiment to make up the volume of air withdrawn by the instruments.

Data and Materials Availability. All data are available in the text or *SI Appendix*.

ACKNOWLEDGMENTS. This work was supported by National Natural Science Foundation of China Grants 91544214 and 21677002; National Key Research and Development Program of China Grant 2016YFC0202000: Task 3; National Research Program for Key Issues in Air Pollution Control Grant DQGG0103; and Robert A. Welch Foundation Grant A-1417. We thank Don Collins for the application of the QUALITY chamber.

1. R. Zhang, A. Khalizov, L. Wang, M. Hu, W. Xu, Nucleation and growth of nanoparticles in the atmosphere. *Chem. Rev.* **112**, 1957–2011 (2012).
2. S. Guo *et al*., Elucidating severe urban haze formation in China. *Proc. Natl. Acad. Sci. U.S.A.* **111**, 17373–17378 (2014).
3. D. Yue *et al*., The roles of sulfuric acid in NPF and growth in the megacity of Beijing. *Atmos. Chem. Phys.* **10**, 4953–4960 (2010).
4. Y. Yu, R. Turco, From molecular clusters to nanoparticles: Role of ambient ionization in tropospheric aerosol formation. *J. Geophys. Res. Atmos.* **106**, 4797–4814 (2001).
5. J. H. Seinfeld, S. N. Pandis, *Atmospheric Chemistry and Physics: From Air Pollution to Climate Change* (John Wiley & Sons, 2016).
6. C. Qiu, R. Zhang, Multiphase chemistry of atmospheric amines. *Phys. Chem. Chem. Phys.* **15**, 5738–5752 (2013).
7. J. Merikanto, D. V. Spracklen, G. W. Mann, S. J. Pickering, K. S. Carslaw, Impact of nucleation on global CCN. *Atmos. Chem. Phys.* **9**, 8601–8616 (2009).
8. R. Zhang *et al*., Formation of urban fine particulate matter. *Chem. Rev.* **115**, 3803–3855 (2015).
9. R. McGraw, R. Zhang, Multivariate analysis of homogeneous nucleation rate measurements. Nucleation in the p-toluic acid/sulfuric acid/water system. *J. Chem. Phys.* **128**, 064508 (2008).
10. Y. Wang *et al*., Assessing the effects of anthropogenic aerosols on Pacific storm track using a multiscale global climate model. *Proc. Natl. Acad. Sci. U.S.A.* **111**, 6894–6899 (2014).
11. J. Fan *et al*., Substantial convection and precipitation enhancements by ultrafine aerosol particles. *Science* **359**, 411–418 (2018).
12. Intergovernmental Panel on Climate Change, *Climate Change 2013: The Physical Science Basis* (Cambridge University Press, 2013).
13. K. A. Rychlik *et al*., In utero ultrafine particulate matter exposure causes offspring pulmonary immunosuppression. *Proc. Natl. Acad. Sci. U.S.A.* **116**, 3443–3448 (2019).
14. G. Wu *et al*., Adverse organogenesis and predisposed long-term metabolic syndrome from prenatal exposure to fine particulate matter. *Proc. Natl. Acad. Sci. U.S.A.* **116**, 11590–11595 (2019).
15. R. Zhang, Atmospheric science. Getting to the critical nucleus of aerosol formation. *Science* **328**, 1366–1367 (2010).
16. Z. B. Wang *et al*., Evaluation on the role of sulfuric acid in the mechanisms of NPF for Beijing case. *Atmos. Chem. Phys.* **11**, 12663–12671 (2011).
17. R. Zhang *et al*., Atmospheric new particle formation enhanced by organic acids. *Science* **304**, 1487–1490 (2004).
18. J. Zhao, A. Khalizov, R. Zhang, R. McGraw, Hydrogen-bonding interaction in molecular complexes and clusters of aerosol nucleation precursors. *J. Phys. Chem. A* **113**, 680–689 (2009).
19. F. Yu, R. Turco, Case studies of particle formation events observed in boreal forests: Implications for nucleation mechanisms. *Atmos. Chem. Phys.* **8**, 6085–6102 (2008).
20. R. Zhang *et al*., Formation of nanoparticles of blue haze enhanced by anthropogenic pollution. *Proc. Natl. Acad. Sci. U.S.A.* **106**, 17650–17654 (2009).
21. A. B. Nadykto, F. Yu, Strong hydrogen bonding between atmospheric nucleation precursors and common organics. *Chem. Phys. Lett.* **435**, 14–18 (2007).
22. L. Yao *et al*., Atmospheric NPF from sulfuric acid and amines in a Chinese megacity. *Science* **361**, 278–281 (2018).
23. J. Wildt *et al*., Suppression of NPF from monoterpene oxidation by NOx. *Atmos. Chem. Phys.* **14**, 2789–2804 (2014).
24. A. Kiendler-Scharr *et al*., NPF in forests inhibited by isoprene emissions. *Nature* **461**, 381–384 (2009).
25. J. Peng *et al*., Markedly enhanced absorption and direct radiative forcing of black carbon under polluted urban environments. *Proc. Natl. Acad. Sci. U.S.A.* **113**, 4266–4271 (2016).
26. J. F. Peng *et al*., Ageing and hygroscopicity variation of black carbon particles in Beijing measured by a quasi-atmospheric aerosol evolution study (QUALITY) chamber. *Atmos. Chem. Phys.* **17**, 10333–10348 (2017).
27. J. F. Peng *et al*., Gasoline aromatics: A critical determinant of urban secondary organic aerosol formation. *Atmos. Chem. Phys.* **17**, 10743–10752 (2017).
28. J. Zheng *et al*., Measurements of gaseous H_2SO_4 by AP-ID-CIMS during CAREBeijing 2008 campaign. *Atmos. Chem. Phys.* **11**, 7755–7765 (2011).
29. J. Zhao, R. Zhang, K. Misaw, K. Shibuy, Experimental product study of the OH-initiated oxidation of m-xylene. *J. Photoch. Photobio. A* **176**, 199–207 (2005).
30. M. E. Levy *et al*., Measurements of submicron aerosols in Houston, Texas during the 2009 SHARP field campaign. *J. Geophys. Res. Atmos.* **118**, 10518–10534 (2013).
31. L. Y. He *et al*., Submicron aerosol analysis and organic source apportionment in an urban atmosphere in Pearl River Delta of China using high-resolution aerosol mass spectrometry. *J. Geophys. Res. Atmos.* **116**, D12304 (2011).
32. Y. Ji *et al*., Reassessing the atmospheric oxidation mechanism of toluene. *Proc. Natl. Acad. Sci. U.S.A.* **114**, 8169–8174 (2017).
33. J. Zheng, A. Khalizov, L. Wang, R. Zhang, Atmospheric pressure-ion drift chemical ionization mass spectrometry for detection of trace gas species. *Anal. Chem.* **82**, 7302–7308 (2010).
34. S.-H. Lee *et al*., NPF in the atmosphere: From molecular clusters to global climate. *J. Geophys. Res. Atmos.* **124**, 7098–7146 (2019).
35. H. Xue, A. F. Khalizov, L. Wang, J. Zheng, R. Zhang, Effects of coating of dicarboxylic acids on the mass-mobility relationship of soot particles. *Environ. Sci. Technol.* **43**, 2787–2792 (2009).
36. H. Xue, A. F. Khalizov, L. Wang, J. Zheng, R. Zhang, Effects of dicarboxylic acid coating on the optical properties of soot. *Phys. Chem. Chem. Phys.* **11**, 7869–7875 (2009).
37. A. F. Khalizov *et al*., Formation of highly hygroscopic soot aerosols upon internal mixing with sulfuric acid vapor. *J. Geophys. Res. Atmos.* **114**, D05208 (2009).
38. M. Wang *et al*., Use of a mobile laboratory to evaluate changes in on-road air pollutants during the Beijing 2008 summer Olympics. *Atmos. Chem. Phys.* **9**, 8247–8263 (2009).